arXiv:2310.00089

Spectral Retrieval with JWST Photometric data: a Case Study for HIP 65426 b

JI WANG (王吉) [1]

[1]Department of Astronomy, The Ohio State University, 100 W 18th Ave, Columbus, OH 43210 USA

Speaker： 闫冰

Date ： 2023/11/24

CONTENT

Introduction

1. Intruction

Directly-imaged exoplanets provide a unique window to understand **atmospheric structure and chemistry**.
This information shed light on the formation pathway and evolution history.
Chemical composition is best studied with spectroscopy whereby spectral lines or bands are resolved and chemical abundances can be measured.
Conventionally, spectroscopic data come from ground-based low-to-medium resolution (R<5000) integral field unit (IFU)
Now, JWST Early Release Science (ERS) program has given us a glimpse of the opportunities and challenges in modeling and interpreting atmospheres with JWST data.
Not every object will receive spectroscopic observations.

1. Introduction

This work attempts to address to what extent one can characterize planetary atmospheres with **JWST photometric data points** in conjunction with **archival ground-based low-spectral resolution data**.

HIP 65426 b—a JWST target in the Early Release Science (ERS) program
photometric data from JWST/NIRCam and MIRI **(~2-16 μm)** and VLT/SPHERE-IRDIS **(~1-2.5 μm)**
spectral data from VLT/SPHERE-IFS **(~1-1.65 μm)**

Retrieval framework

2 Retrieval framework

They model **exoplanet atmospheres** based on petitRADTRANS and consider both low and high resolution modes (R=1,000 and R=1,000,000) when such data are available.
For the **temperature profile**, they adopt a flexible P-T profile as described in Petit dit de la Roche et al. (2020).
To **sample the posterior distribution in a Bayesian framework**, they used PyMultiNest (Buchner et al. 2014).

We include **MgSiO3 clouds** (Molli`ere et al. 2020) with a new addition of featureless extinction.
The extinction τ follows the exponential relation with wavelength (λ) such that $\boldsymbol{\tau(\lambda) = exp(-\alpha \cdot \frac{1\,\mu m}{\lambda})}$ (Gordon et al. 2003), where α is the extinction coefficient.

A full list of parameters and their priors are in Table 1.

Table 1. Parameters used in retrieval and their priors.

Parameter	Unit	Type	Lower or Mean	Upper or Std
Surface Gravity ($\log(g)$)	cgs	Uniform	2.5	5.5
Planet Radius (R_P)	M_{Jupiter}	Uniform	0.5	5.0
H_2O Mixing Ratio ($\log(\mathrm{mr}_{H_2O})$)	$\cdots$	Log-uniform	-10	-1
CO Mixing Ratio ($\log(\mathrm{mr}_{CO})$)	$\cdots$	Log-uniform	-10	-1
CO_2 Mixing Ratio ($\log(\mathrm{mr}_{CO_2})$)	$\cdots$	Log-uniform	-10	-1
CH_4 Mixing Ratio ($\log(\mathrm{mr}_{CH_4})$)	$\cdots$	Log-uniform	-10	-1
Temperature at 3.2 bar (t_{int})	K	Uniform	800	2500
ΔT between 100 and 32 bar	K	Uniform	0	2500
ΔT between 32 and 10 bar	K	Uniform	0	2000
ΔT between 10 and 3.2 bar	K	Uniform	0	1500
ΔT between 3.2 and 1 bar	K	Uniform	0	1000
ΔT between 1 and 0.1 bar	K	Uniform	0	1000
ΔT between 0.1 bar and 1 mbar	K	Uniform	0	1000
ΔT between 1 mbar and 10 nbar	K	Uniform	0	1000
$MgSiO_3$ Mixing Ratio ($\log(\mathrm{mr}_{MgSiO_3})$)	$\cdots$	Log-uniform	-10	-1
Vertical diffusion coefficient ($\log(K_{zz})$)	$cm2 \cdot s^{-1}$	Log-uniform	5	10
$v_{\mathrm{settling}}/v_{\mathrm{mixing}}$ (f_{sed})	$\cdots$	Uniform	0	5
Width of log-normal particle size distribution (σ_g)	$\cdots$	Uniform	1.05	3.05
Extinction coefficient (α)	$\cdots$	Uniform	0.0	5.0

Testing with mock data

PART.03

3 Testing with mock data

3.1 Generating mock data

To generate model spectra, we use the model parameters listed in the "Input" column of Table 2.
Four cases are considered in terms of **metallicity (1x and 10x solar)** and **the mixing ratio of MgSiO$_3$ (low at -4 dex and high at -3 dex).**

Table 2. Input and Retrieved Parameters Using Mock Data.

Parameter	Unit	1x solar		10x solar		All Varying		Input
MgSiO$_3$		low*	high	low	high	varying		
$\log(g)$	cgs	$4.03^{+0.03}_{-0.02}$	$3.99^{+0.12}_{-0.06}$	$4.14^{+0.11}_{-0.12}$	$3.39^{+0.16}_{-0.12}$	$3.17^{+0.08}_{-0.13}$	$4.33^{+0.24}_{-0.22}$	4.0
R_P	R_{Jupiter}	$3.53^{+0.01}_{-0.01}$	$3.46^{+0.03}_{-0.02}$	$3.54^{+0.02}_{-0.02}$	$3.38^{+0.03}_{-0.03}$	3.50	$2.89^{+0.06}_{-0.06}$	3.5
$\log(mr_{H_2O})$	$\cdots$	-2.605		-1.655		$-2.635^{+0.031}_{-0.040}$	$-2.549^{+0.142}_{-0.143}$	-2.605 or -1.655
$\log(mr_{CO})$	$\cdots$	-2.258		-1.303		$-2.169^{+0.126}_{-0.111}$	$-2.051^{+0.331}_{-0.300}$	-2.258 or -1.303
$\log(mr_{CO_2})$	$\cdots$	-6.300		-4.337		$-8.575^{+0.910}_{-0.837}$	$-8.420^{+1.019}_{-0.950}$	-6.300 or -4.337
$\log(mr_{CH_4})$	$\cdots$	-5.669		-5.661		$-5.905^{+0.105}_{-0.280}$	$-7.342^{+1.205}_{-1.598}$	-5.669 or -5.661
t_{int}	K	1795^{+54}_{-70}	1771^{+75}_{-77}	1838^{+102}_{-128}	2349^{+95}_{-137}	1677^{+69}_{-70}	1618^{+72}_{-102}	1800
ΔT between 100 and 32 bar	K	1512^{+639}_{-630}	1860^{+471}_{-926}	1374^{+769}_{-891}	1254^{+831}_{-845}	1765^{+462}_{-669}	2107^{+274}_{-459}	2000
ΔT between 32 and 10 bar	K	1639^{+249}_{-290}	1776^{+161}_{-282}	1237^{+501}_{-646}	1089^{+613}_{-717}	1691^{+190}_{-269}	1501^{+310}_{-372}	1500
ΔT between 10 and 3.2 bar	K	954^{+196}_{-153}	985^{+305}_{-343}	541^{+332}_{-241}	1082^{+296}_{-469}	631^{+260}_{-225}	176^{+257}_{-124}	1000
ΔT between 3.2 and 1 bar	K	517^{+86}_{-108}	331^{+118}_{-111}	715^{+117}_{-156}	845^{+95}_{-132}	330^{+101}_{-104}	168^{+167}_{-107}	500
ΔT between 1 and 0.1 bar	K	479^{+72}_{-59}	687^{+75}_{-77}	311^{+66}_{-50}	553^{+45}_{-44}	475^{+73}_{-66}	496^{+196}_{-195}	500
ΔT between 0.1 bar and 1 mbar	K	547^{+260}_{-250}	360^{+272}_{-214}	766^{+150}_{-187}	618^{+62}_{-60}	543^{+257}_{-282}	540^{+288}_{-331}	500
ΔT between 1 mbar and 10 nbar	K	511^{+332}_{-338}	515^{+324}_{-341}	473^{+351}_{-319}	543^{+308}_{-348}	514^{+285}_{-302}	512^{+296}_{-304}	500
$\log(mr_{MgSiO_3})$	$\cdots$	-4	-3	-4	-3	$-3.36^{+0.11}_{-0.23}$	$-4.07^{+0.68}_{-2.90}$	-4 or -3
$\log(K_{zz})$	cm2·s^{-1}			8.0			$8.04^{+0.98}_{-1.10}$	8.0
f_{sed}	$\cdots$			1.3			$3.36^{+0.97}_{-1.34}$	1.3
Cloud log-normal size σ_g	$\cdots$			1.31			$2.06^{+0.56}_{-0.56}$	1.31
Extinction coefficient α	$\cdots$	$3.10^{+0.05}_{-0.05}$	$3.34^{+0.16}_{-0.16}$	$2.99^{+0.22}_{-0.23}$	$2.53^{+0.32}_{-0.26}$	$2.96^{+0.23}_{-0.14}$	$3.62^{+0.29}_{-0.25}$	3.0
C/O	$\cdots$	0.55	0.55	0.55	0.55	$0.65^{+0.05}_{-0.05}$	$0.66^{+0.09}_{-0.10}$	0.55

NOTE—∗: Low, high, and varying refer to cases with low (-4), high (-3), and varying mixing ratio for MgSiO3; see §3.2 for more details of each case (or column).

3 Testing with mock data

3.1 Generating mock data

To simulate the mock data, we resample a model spectrum to the wavelength grid of existing data.
Table 3 tabulates the data set including **VLT/SPHERE-IFS between 1.00 and 1.65 μm** (Chauvin et al. 2017), **VLT/SPHERE-IRDIS H and K-band photometry** (Cheetham et al. 2019), and **JWST NIRCam and MIRI photometry** (Carter et al. 2023).

Since the spectral resolution of low-resolution data is not uniform across the wavelength range, sampling the synthetic spectrum to the wavelength grid of existing data ensures that the synthetic spectrum has the same varying spectral resolution as the original spectrum.
For JWST photometric points, we convolve the response profile of each filter (Rodrigo & Solano 2020) with the model spectrum to compare to the data.

Table 3. Joint Data for JWST and SPHERE

Filter*	λ_0	$\Delta\lambda$	flux
	[μm]	[μm]	[W/m/μm]
H2	1.588	0.053	$8.57 \pm 0.38 \times 10^{-17}$
H3	1.667	0.055	$10.13 \pm 0.56 \times 10^{-17}$
K1	2.102	0.102	$7.50 \pm 0.60 \times 10^{-17}$
K2	2.255	0.109	$7.10 \pm 0.60 \times 10^{-17}$
F250M	2.500	0.180	$4.29 \pm 0.33 \times 10^{-17}$
F300M	2.990	0.310	$2.89 \pm 0.20 \times 10^{-17}$
F356M	3.560	0.780	$3.36 \pm 0.23 \times 10^{-17}$
F410M	4.090	0.430	$2.49 \pm 0.18 \times 10^{-17}$
F444M	4.420	1.020	$1.97 \pm 0.13 \times 10^{-17}$
F1140C	11.300	1.600	$7.40 \pm 1.16 \times 10^{-19}$
F1550C	15.500	1.800	$2.74 \pm 0.46 \times 10^{-19}$
	1.002	0.011	$2.43 \pm 0.57 \times 10^{-17}$
	1.011	0.011	$3.15 \pm 0.67 \times 10^{-17}$
	1.021	0.011	$3.56 \pm 0.57 \times 10^{-17}$
	1.030	0.011	$3.20 \pm 0.43 \times 10^{-17}$
	1.040	0.011	$4.09 \pm 0.48 \times 10^{-17}$
	1.050	0.011	$3.83 \pm 0.43 \times 10^{-17}$
	1.060	0.011	$4.15 \pm 0.49 \times 10^{-17}$
	1.070	0.011	$4.46 \pm 0.52 \times 10^{-17}$
	1.081	0.011	$4.68 \pm 0.43 \times 10^{-17}$
	1.091	0.011	$5.14 \pm 0.48 \times 10^{-17}$
	1.102	0.011	$4.75 \pm 0.54 \times 10^{-17}$
	1.112	0.011	$5.13 \pm 0.58 \times 10^{-17}$
	1.123	0.011	$4.78 \pm 0.64 \times 10^{-17}$
	1.133	0.011	$5.23 \pm 0.68 \times 10^{-17}$

Table 3 *(continued)*

Filter*	λ_0	$\Delta\lambda$	flux
	[μm]	[μm]	[W/m/μm]
	1.140	0.019	$3.91 \pm 0.40 \times 10^{-17}$
	1.159	0.019	$4.13 \pm 0.42 \times 10^{-17}$
	1.178	0.019	$4.64 \pm 0.45 \times 10^{-17}$
	1.197	0.019	$5.37 \pm 0.54 \times 10^{-17}$
	1.216	0.019	$6.36 \pm 0.57 \times 10^{-17}$
	1.235	0.019	$6.76 \pm 0.60 \times 10^{-17}$
	1.255	0.019	$7.11 \pm 0.62 \times 10^{-17}$
	1.274	0.019	$7.23 \pm 0.63 \times 10^{-17}$
	1.294	0.019	$7.60 \pm 0.67 \times 10^{-17}$
	1.314	0.019	$7.30 \pm 0.65 \times 10^{-17}$
	1.333	0.019	$6.05 \pm 0.58 \times 10^{-17}$
	1.353	0.019	$5.40 \pm 0.65 \times 10^{-17}$
	1.372	0.019	$5.52 \pm 0.87 \times 10^{-17}$
	1.391	0.019	$5.88 \pm 0.73 \times 10^{-17}$
	1.411	0.019	$5.29 \pm 0.55 \times 10^{-17}$
	1.430	0.019	$4.52 \pm 0.46 \times 10^{-17}$
	1.449	0.019	$4.77 \pm 0.44 \times 10^{-17}$
	1.467	0.019	$5.37 \pm 0.48 \times 10^{-17}$
	1.486	0.019	$5.89 \pm 0.51 \times 10^{-17}$
	1.504	0.019	$5.93 \pm 0.50 \times 10^{-17}$
	1.522	0.019	$6.26 \pm 0.52 \times 10^{-17}$
	1.539	0.019	$6.78 \pm 0.56 \times 10^{-17}$
	1.556	0.019	$7.32 \pm 0.60 \times 10^{-17}$
	1.573	0.019	$7.56 \pm 0.62 \times 10^{-17}$
	1.589	0.019	$8.04 \pm 0.67 \times 10^{-17}$
	1.605	0.019	$8.50 \pm 0.71 \times 10^{-17}$
	1.621	0.019	$8.58 \pm 0.71 \times 10^{-17}$
	1.636	0.019	$9.01 \pm 0.76 \times 10^{-17}$
	0.000	0.000	$0.00 \pm 0.00 \times 10^{-17}$

NOTE—*: H and K photometric data are from Cheetham et al. (2019); JWST photometric data (beginning with "F") are from Carter et al. (2023); rows without a filter name are data from SPHERE integrated field unit (Chauvin et al. 2017).

3 Testing with mock data
3.2 Analyzing mock data

We start with a more constraining condition in which we fix chemical abundance to 1x or 10x solar and cloud properties.
We then relax some constraints to allow for the variation of mixing ratios for molecules and the cloud species MgSiO3.
We fix planet radius at the input value of **3.5 R$_{Jupiter}$** and fix chemical abundance to **1x solar metallicity**.
Lastly, we allow all parameters to vary.

Table 2. Input and Retrieved Parameters Using Mock Data.

Parameter	Unit	1x solar		10x solar		All Varying		Input
MgSiO$_3$		low*	high	low	high	varying		
$\log(g)$	cgs	$4.03^{+0.03}_{-0.02}$	$3.99^{+0.12}_{-0.06}$	$4.14^{+0.11}_{-0.12}$	$3.39^{+0.16}_{-0.12}$	$3.17^{+0.08}_{-0.13}$	$4.33^{+0.24}_{-0.22}$	4.0
R_P	R$_{Jupiter}$	$3.53^{+0.01}_{-0.01}$	$3.46^{+0.03}_{-0.02}$	$3.54^{+0.02}_{-0.02}$	$3.38^{+0.03}_{-0.03}$	3.50	$2.89^{+0.06}_{-0.06}$	3.5
$\log(mr_{H_2O})$	$\cdots$	-2.605		-1.655		$-2.635^{+0.031}_{-0.040}$	$-2.549^{+0.142}_{-0.143}$	-2.605 or -1.655
$\log(mr_{CO})$	$\cdots$	-2.258		-1.303		$-2.169^{+0.126}_{-0.111}$	$-2.051^{+0.331}_{-0.300}$	-2.258 or -1.303
$\log(mr_{CO_2})$	$\cdots$	-6.300		-4.337		$-8.575^{+0.910}_{-0.837}$	$-8.420^{+1.019}_{-0.950}$	-6.300 or -4.337
$\log(mr_{CH_4})$	$\cdots$	-5.669		-5.661		$-5.905^{+0.105}_{-0.280}$	$-7.342^{+1.205}_{-1.598}$	-5.669 or -5.661
t_{int}	K	1795^{+54}_{-70}	1771^{+75}_{-77}	1838^{+102}_{-128}	2349^{+95}_{-137}	1677^{+69}_{-70}	1618^{+72}_{-102}	1800
ΔT between 100 and 32 bar	K	1512^{+639}_{-630}	1860^{+471}_{-926}	1374^{+769}_{-891}	1254^{+831}_{-845}	1765^{+462}_{-669}	2107^{+274}_{-459}	2000
ΔT between 32 and 10 bar	K	1639^{+249}_{-290}	1776^{+161}_{-282}	1237^{+501}_{-646}	1089^{+613}_{-717}	1691^{+190}_{-269}	1501^{+310}_{-372}	1500
ΔT between 10 and 3.2 bar	K	954^{+196}_{-153}	985^{+305}_{-343}	541^{+332}_{-241}	1082^{+296}_{-469}	631^{+260}_{-225}	176^{+257}_{-124}	1000
ΔT between 3.2 and 1 bar	K	517^{+86}_{-108}	331^{+118}_{-111}	715^{+117}_{-156}	845^{+95}_{-132}	330^{+101}_{-104}	168^{+167}_{-107}	500
ΔT between 1 and 0.1 bar	K	479^{+72}_{-59}	687^{+75}_{-77}	311^{+66}_{-50}	553^{+45}_{-44}	475^{+73}_{-66}	496^{+196}_{-195}	500
ΔT between 0.1 bar and 1 mbar	K	547^{+260}_{-250}	360^{+272}_{-214}	766^{+150}_{-187}	618^{+62}_{-60}	543^{+257}_{-282}	540^{+288}_{-331}	500
ΔT between 1 mbar and 10 nbar	K	511^{+332}_{-338}	515^{+324}_{-341}	473^{+351}_{-319}	543^{+308}_{-348}	514^{+285}_{-302}	512^{+296}_{-304}	500
$\log(mr_{MgSiO_3})$	$\cdots$	-4	-3	-4	-3	$-3.36^{+0.11}_{-0.23}$	$-4.07^{+0.68}_{-2.90}$	-4 or -3
$\log(K_{zz})$	cm2·s^{-1}			8.0			$8.04^{+0.98}_{-1.10}$	8.0
f_{sed}	$\cdots$			1.3			$3.36^{+0.97}_{-1.34}$	1.3
Cloud log-normal size σ_g	$\cdots$			1.31			$2.06^{+0.56}_{-0.56}$	1.31
Extinction coefficient α	$\cdots$	$3.10^{+0.05}_{-0.05}$	$3.34^{+0.16}_{-0.16}$	$2.99^{+0.22}_{-0.23}$	$2.53^{+0.32}_{-0.26}$	$2.96^{+0.23}_{-0.14}$	$3.62^{+0.29}_{-0.25}$	3.0
C/O	$\cdots$	0.55	0.55	0.55	0.55	$0.65^{+0.05}_{-0.05}$	$0.66^{+0.09}_{-0.10}$	0.55

NOTE—*: Low, high, and varying refer to cases with low (-4), high (-3), and varying mixing ratio for MgSiO$_3$; see §3.2 for more details of each case (or column).

3.3 Lessons learned from mock data

Summarize what has been learned from the exercise of retrieving on mock data:
- In the absence of modeling systematics, we are able to constrain the mixing ratio for molecular species, cloud species $MgSiO_3$, and the extinction coefficient α to describe a featureless spectral slope.
- In more constraining cases in which molecular species are fixed to chemical equilibrium values and/or some cloud parameters are fixed, typical uncertainties for $MgSiO_3$ and α are 0.2 dex and 0.1-0.3 dex, respectively.
- Planet properties such as surface gravity and planet radius are generally retrieved within 0.1 dex and 0.05 $R_{Jupiter}$ for constraining cases in which molecular species are fixed. However, **retrieved planet properties are unreliable when chemical abundances become free parameters in retrievals.**
- By comparing the "all varying" case of 1x solar metallicity and the case where abundances are fixed at 10x solar metallicity, we can distinguish between 1x and 10x solar metallicity cases at 3-σ level using CO and 6-σ level using H_2O.
- By comparing C/O ratios between fixed and varying cases, the C/O has a typical error bar of 0.1 and a upward bias of ~0.1.

Retrievals on SPHERE+JWST joint data

joint data

PART.04

4 Retrievals on SPHERE+JWST joint data
4.1 Solar metallicity and C/O<1 for HIP 65426 b

We perform retrieval analyses for the joint data set of SPHERE and JWST data with different combination of C/O ratios (0.40, 0.55, and 1.00) and metallicities (1x and 10x solar). We also run retrieval by varying all parameters. The results are given in Table 4.

By comparing Bayesian evidence (EV), the retrieval model using sub-solar C/O (C/O = 0.40) and solar metallicity has the highest Bayesian evidence. The next most preferred model using solar C/O (C/O = 0.55) and solar metallicity has a differential natural log evidence (Δln(EV) of -1.47). Therefore, the data can be explained by a model with **1x solar metallicity and two C/O ratios at 0.40 and 0.55.**

Other models are strongly disfavored.

Table 4. Retrieved Parameters Using Real Data.

Parameter	Unit	C/O = 0.40		C/O = 0.55		C/O = 1.00		
Solar Metallicity		1x	10x	1x	10x	1x	10x	All Varying
$\log(g)$	cgs	$3.19^{+0.23}_{-0.25}$	$3.41^{+0.19}_{-0.25}$	$3.03^{+0.21}_{-0.21}$	$3.57^{+0.15}_{-0.15}$	$2.63^{+0.12}_{-0.08}$	$2.60^{+0.09}_{-0.06}$	$2.60^{+0.09}_{-0.06}$
R_P	$R_{Jupiter}$	$1.23^{+0.02}_{-0.02}$	$1.23^{+0.02}_{-0.02}$	$1.25^{+0.02}_{-0.02}$	$1.25^{+0.02}_{-0.02}$	$1.18^{+0.03}_{-0.02}$	$1.14^{+0.02}_{-0.02}$	$1.18^{+0.01}_{-0.01}$
$\log(mr_{H_2O})$	...	-2.311	-1.366	-2.605	-1.655	-4.314	-3.994	$-1.10^{+0.06}_{-0.09}$
$\log(mr_{CO})$	...	-2.259	-1.312	-2.258	-1.303	-2.290	-1.322	$-5.91^{+2.45}_{-2.30}$
$\log(mr_{CO_2})$	...	-5.988	-4.036	-6.300	-4.337	-8.954	-7.475	$-7.23^{+1.41}_{-1.45}$
$\log(mr_{CH_4})$	...	-5.913	-5.957	-5.669	-5.661	-3.913	-3.331	$-7.10^{+1.73}_{-1.58}$
t_{int}	K	1853^{+38}_{-38}	1906^{+115}_{-71}	1842^{+34}_{-36}	1849^{+70}_{-41}	2487^{+8}_{-21}	2485^{+9}_{-21}	2244^{+141}_{-165}
ΔT between 100 and 32 bar	K	1206^{+742}_{-720}	1212^{+633}_{-614}	1042^{+711}_{-587}	1238^{+712}_{-667}	945^{+655}_{-525}	905^{+763}_{-514}	1281^{+670}_{-689}
ΔT between 32 and 10 bar	K	300^{+556}_{-215}	1122^{+502}_{-606}	257^{+555}_{-181}	539^{+532}_{-335}	173^{+164}_{-103}	302^{+276}_{-183}	1015^{+544}_{-546}
ΔT between 10 and 3.2 bar	K	68^{+167}_{-48}	467^{+448}_{-274}	61^{+150}_{-44}	163^{+299}_{-117}	45^{+40}_{-27}	67^{+57}_{-40}	666^{+425}_{-385}
ΔT between 3.2 and 1 bar	K	37^{+51}_{-24}	89^{+103}_{-54}	42^{+54}_{-26}	56^{+99}_{-40}	8^{+11}_{-5}	11^{+14}_{-7}	265^{+163}_{-141}
ΔT between 1 and 0.1 bar	K	112^{+86}_{-79}	26^{+24}_{-16}	142^{+97}_{-84}	45^{+48}_{-27}	306^{+61}_{-65}	94^{+39}_{-49}	86^{+100}_{-56}
ΔT between 0.1 bar and 1 mbar	K	882^{+66}_{-80}	562^{+98}_{-127}	870^{+67}_{-75}	797^{+81}_{-79}	620^{+65}_{-59}	638^{+49}_{-34}	231^{+52}_{-62}
ΔT between 1 mbar and 10 nbar	K	493^{+290}_{-280}	759^{+135}_{-207}	475^{+299}_{-269}	591^{+237}_{-292}	145^{+111}_{-74}	220^{+66}_{-64}	954^{+30}_{-54}
$\log(mr_{MgSiO_3})$	...	$-2.56^{+0.56}_{-0.55}$	$-1.92^{+0.36}_{-0.31}$	$-3.38^{+0.37}_{-0.39}$	$-2.10^{+0.54}_{-0.61}$	$-1.64^{+0.34}_{-0.36}$	$-1.25^{+0.14}_{-0.25}$	$-1.62^{+0.35}_{-0.58}$
$\log(K_{zz})$	cm2·s^{-1}	$5.49^{+0.29}_{-0.22}$	$6.10^{+0.28}_{-0.18}$	$5.48^{+0.21}_{-0.16}$	$5.56^{+0.24}_{-0.22}$	$7.40^{+0.26}_{-0.21}$	$8.42^{+0.26}_{-0.28}$	$7.38^{+0.19}_{-0.24}$
f_{sed}	...	$0.63^{+0.23}_{-0.21}$	$0.41^{+0.15}_{-0.11}$	$0.44^{+0.16}_{-0.13}$	$0.51^{+0.20}_{-0.20}$	$0.31^{+0.12}_{-0.11}$	$0.16^{+0.06}_{-0.04}$	$0.36^{+0.09}_{-0.12}$
Cloud log-normal size σ_g	...	$1.22^{+0.19}_{-0.10}$	$1.29^{+0.34}_{-0.14}$	$1.21^{+0.20}_{-0.09}$	$1.26^{+0.33}_{-0.14}$	$1.21^{+0.15}_{-0.09}$	$1.22^{+0.18}_{-0.10}$	$1.21^{+0.36}_{-0.11}$
Extinction coefficient α	...	$0.06^{+0.05}_{-0.04}$	$0.05^{+0.04}_{-0.03}$	$0.07^{+0.05}_{-0.03}$	$0.07^{+0.05}_{-0.04}$	$2.09^{+0.22}_{-0.14}$	$2.24^{+0.18}_{-0.12}$	$0.03^{+0.03}_{-0.02}$
$\ln(EV)$		0.00	-23.76	-1.47	-15.86	-304.19	-365.29	-20.43
$\log(L/L_\odot)$		$-4.167^{+0.003}_{-0.002}$	$-4.160^{+0.003}_{-0.003}$	$-4.168^{+0.003}_{-0.002}$	$-4.164^{+0.002}_{-0.003}$	$-4.160^{+0.003}_{-0.003}$	$-4.158^{+0.004}_{-0.002}$	$-4.158^{+0.003}_{-0.002}$
T_{eff}	K	1477^{+8}_{-10}	1480^{+12}_{-11}	1463^{+10}_{-7}	1464^{+10}_{-12}	1515^{+14}_{-15}	1540^{+9}_{-15}	1511^{+7}_{-8}

4.2 Strong evidence of silicate clouds

- All retrievals return a mixing ratio for MgSiO3 that is at least -3.4, a value that we can confidently detect for mock data (§3).
- The dip in the 11.4 µm photometry (Fig. 1) is another visual evidence for the silicate clouds.
- The peak pressure levels (~0.1 bar to 5 mbar) of the spectrally-averaged contribution function overlaps with that of the cloud opacity distribution (Fig. 2).
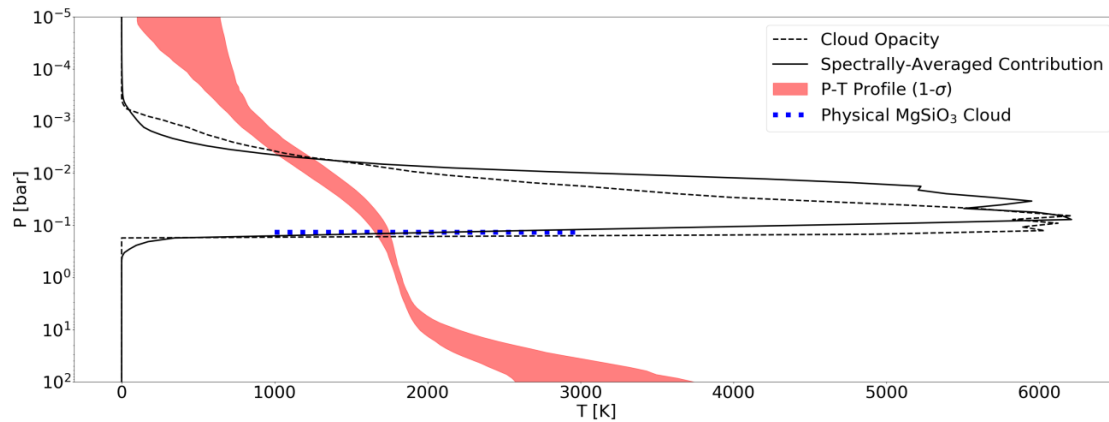
Figure 2. Retrieved P-T profile (1-σ region in red shaded region) for HIP 65426 b (assuming 1x solar metallcity and C/O=0.4) The spectrally-averaged contribution function is shown as the black solid line, which completely overlaps with retrieved cloud layer (black dashed line). The pressure level of the retrieved cloud layer is consistent with that of a physical MgSiO$_3$ cloud (blue dotted line). More results with other assumptions can be found in Table 4.
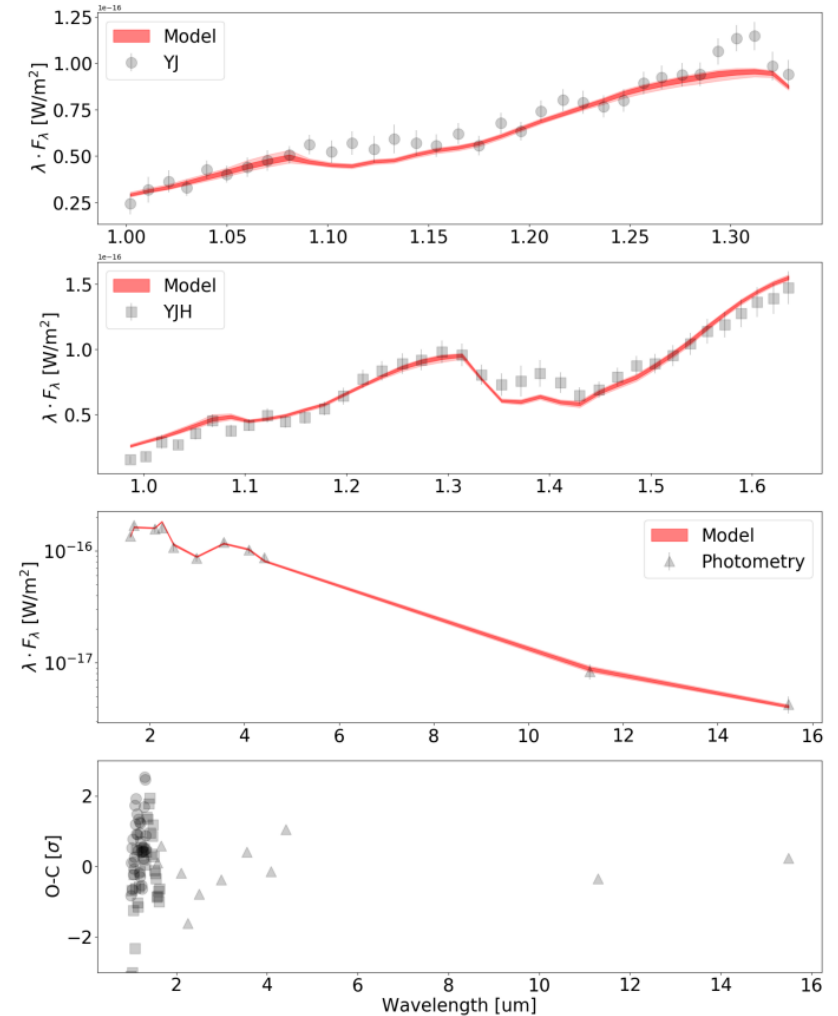
Figure 1. Retrieved spectra for HIP 65426 b (assuming 1x solar metallcity and C/O=0.4). Top three panels are the observed spectroscopic and photometric data (black) and the 1-σ (16 to 84 percentile, darker red) and 2-σ (2.5 to 97.5 percentile, lighter red) distribution of modeled spectra. The bottom panel is a residual plot with data minus model and divided by the individual errors. More results with other assumptions can be found in Table 4.

4 Retrievals on SPHERE+JWST joint data
4.3 No Evidence of featureless dust extinction

We would like to investigate the possibility of HIP 65426 b processing an enshrouding dust that produces a featureless extinction spectral slope, similar to that as inferred from the PDS 70 planets (Wang et al. 2021). We do not find any evidence of such an enshrouding dust.

It is not surprising to find a zero α because of the older age of HIP 65426 b(14±4 Myr) than PDS 70 b and c(5-8 Myr). HIP 65426 b may have already ceased the accretion and the dust has already settled a few Myrs after the active accretion.

Table 4. Retrieved Parameters Using Real Data.

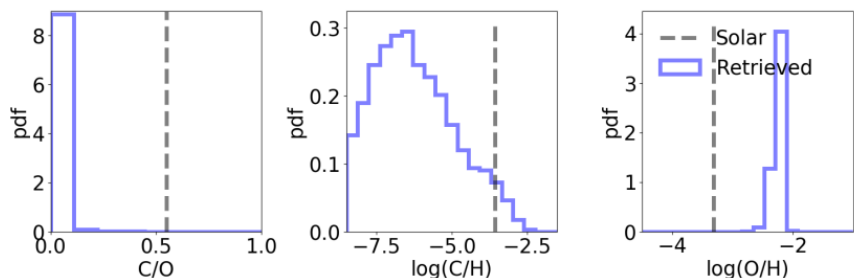| Parameter	Unit	C/O = 0.40		C/O = 0.55		C/O = 1.00		
Solar Metallicity		1x	10x	1x	10x	1x	10x	**All Varying**
$\log(g)$	cgs	$3.19^{+0.23}_{-0.25}$	$3.41^{+0.19}_{-0.25}$	$3.03^{+0.21}_{-0.21}$	$3.57^{+0.15}_{-0.15}$	$2.63^{+0.12}_{-0.08}$	$2.60^{+0.09}_{-0.06}$	$2.60^{+0.09}_{-0.06}$
R_P	$R_{Jupiter}$	$1.23^{+0.02}_{-0.02}$	$1.23^{+0.02}_{-0.02}$	$1.25^{+0.02}_{-0.02}$	$1.25^{+0.02}_{-0.02}$	$1.18^{+0.03}_{-0.02}$	$1.14^{+0.02}_{-0.02}$	$1.18^{+0.01}_{-0.01}$
$\log(mr_{H_2O})$	$\cdots$	-2.311	-1.366	-2.605	-1.655	-4.314	-3.994	$-1.10^{+0.06}_{-0.09}$
$\log(mr_{CO})$	$\cdots$	-2.259	-1.312	-2.258	-1.303	-2.290	-1.322	$-5.91^{+2.45}_{-2.30}$
$\log(mr_{CO_2})$	$\cdots$	-5.988	-4.036	-6.300	-4.337	-8.954	-7.475	$-7.23^{+1.41}_{-1.45}$
$\log(mr_{CH_4})$	$\cdots$	-5.913	-5.957	-5.669	-5.661	-3.913	-3.331	$-7.10^{+1.73}_{-1.58}$
t_{int}	K	1853^{+38}_{-38}	1906^{+115}_{-71}	1842^{+34}_{-36}	1849^{+70}_{-41}	2487^{+8}_{-21}	2485^{+9}_{-21}	2244^{+141}_{-165}
ΔT between 100 and 32 bar	K	1206^{+742}_{-720}	1212^{+633}_{-614}	1042^{+711}_{-587}	1238^{+712}_{-667}	945^{+655}_{-525}	905^{+763}_{-514}	1281^{+670}_{-689}
ΔT between 32 and 10 bar	K	300^{+556}_{-215}	1122^{+502}_{-606}	257^{+555}_{-181}	539^{+532}_{-335}	173^{+164}_{-103}	302^{+276}_{-183}	1015^{+544}_{-546}
ΔT between 10 and 3.2 bar	K	68^{+167}_{-48}	467^{+448}_{-274}	61^{+150}_{-44}	163^{+299}_{-117}	45^{+40}_{-27}	67^{+57}_{-40}	666^{+425}_{-385}
ΔT between 3.2 and 1 bar	K	37^{+51}_{-24}	89^{+103}_{-54}	42^{+54}_{-26}	56^{+99}_{-40}	8^{+11}_{-5}	11^{+14}_{-7}	265^{+163}_{-141}
ΔT between 1 and 0.1 bar	K	112^{+86}_{-79}	26^{+24}_{-16}	142^{+97}_{-84}	45^{+48}_{-27}	306^{+61}_{-65}	94^{+39}_{-49}	86^{+100}_{-56}
ΔT between 0.1 bar and 1 mbar	K	882^{+66}_{-80}	562^{+98}_{-127}	870^{+67}_{-75}	797^{+81}_{-79}	620^{+65}_{-59}	638^{+49}_{-34}	231^{+52}_{-62}
ΔT between 1 mbar and 10 nbar	K	493^{+290}_{-280}	759^{+135}_{-207}	475^{+299}_{-269}	591^{+237}_{-292}	145^{+111}_{-74}	220^{+66}_{-64}	954^{+30}_{-54}
$\log(mr_{MgSiO_3})$	$\cdots$	$-2.56^{+0.56}_{-0.55}$	$-1.92^{+0.36}_{-0.31}$	$-3.38^{+0.37}_{-0.39}$	$-2.10^{+0.54}_{-0.61}$	$-1.64^{+0.34}_{-0.36}$	$-1.25^{+0.14}_{-0.25}$	$-1.62^{+0.35}_{-0.58}$
$\log(K_{zz})$	$cm2 \cdot s^{-1}$	$5.49^{+0.29}_{-0.22}$	$6.10^{+0.28}_{-0.18}$	$5.48^{+0.21}_{-0.16}$	$5.56^{+0.24}_{-0.22}$	$7.40^{+0.26}_{-0.21}$	$8.42^{+0.26}_{-0.28}$	$7.38^{+0.19}_{-0.24}$
f_{sed}	$\cdots$	$0.63^{+0.23}_{-0.21}$	$0.41^{+0.15}_{-0.11}$	$0.44^{+0.16}_{-0.13}$	$0.51^{+0.20}_{-0.20}$	$0.31^{+0.12}_{-0.11}$	$0.16^{+0.06}_{-0.04}$	$0.36^{+0.09}_{-0.12}$
Cloud log-normal size σ_g	$\cdots$	$1.22^{+0.19}_{-0.10}$	$1.29^{+0.34}_{-0.14}$	$1.21^{+0.20}_{-0.09}$	$1.26^{+0.33}_{-0.14}$	$1.21^{+0.15}_{-0.09}$	$1.22^{+0.18}_{-0.10}$	$1.21^{+0.36}_{-0.11}$
Extinction coefficient α	$\cdots$	$0.06^{+0.05}_{-0.04}$	$0.05^{+0.04}_{-0.03}$	$0.07^{+0.05}_{-0.04}$	$0.07^{+0.05}_{-0.04}$	$2.09^{+0.22}_{-0.14}$	$2.24^{+0.18}_{-0.12}$	$0.03^{+0.03}_{-0.02}$
$\ln(EV)$		0.00	-23.76	-1.47	-15.86	-304.19	-365.29	-20.43
$\log(L/L_\odot)$		$-4.167^{+0.003}_{-0.002}$	$-4.160^{+0.003}_{-0.003}$	$-4.168^{+0.003}_{-0.002}$	$-4.164^{+0.002}_{-0.003}$	$-4.160^{+0.003}_{-0.003}$	$-4.158^{+0.004}_{-0.002}$	$-4.158^{+0.003}_{-0.002}$
T_{eff}	K	1477^{+8}_{-10}	1480^{+12}_{-11}	1463^{+10}_{-7}	1464^{+10}_{-12}	1515^{+14}_{-15}	1540^{+9}_{-15}	1511^{+7}_{-8}

4 Retrievals on SPHERE+JWST joint data
4.4 Non–sensible chemical abundances

We find that the retrieved mixing ratios for molecules (Table 4 "All Varying" case) are significantly different from the chemical equilibrium cases that we have considered.

Fig. 3 shows the retrieved C and O abundances and C/O for the all-varying retrieval run. The retrieved C/O is at 0 indicating an abnormally high O and low C abundance. This is driven by the aforementioned high H2O mixing ratio and low CO mixing ratio.

The Bayesian evidence for the all-varying run has a Δln(EV) of -20.43 as compared to the preferred model. Therefore, the all-varying run and the inferred non-physical molecular mixing ratios should be regarded with extremely low confidence.

Figure 3. Retrieved C and O abundances and C/O: C and O abundances from posterior samples are blue histograms, and stellar values are the black dashed lines. Free retrieval by varying all parameters returns non-physical results (e.g., C/O∼0). More details can be found in §4.4.

Table 4. Retrieved Parameters Using Real Data.

Parameter	Unit	C/O = 0.40		C/O = 0.55		C/O = 1.00		
Solar Metallicity		1x	10x	1x	10x	1x	10x	All Varying
$\log(g)$	cgs	$3.19^{+0.23}_{-0.25}$	$3.41^{+0.19}_{-0.25}$	$3.03^{+0.21}_{-0.21}$	$3.57^{+0.15}_{-0.15}$	$2.63^{+0.12}_{-0.08}$	$2.60^{+0.09}_{-0.06}$	$2.60^{+0.09}_{-0.06}$
R_P	$R_{Jupiter}$	$1.23^{+0.02}_{-0.02}$	$1.23^{+0.02}_{-0.02}$	$1.25^{+0.02}_{-0.02}$	$1.25^{+0.02}_{-0.02}$	$1.18^{+0.03}_{-0.02}$	$1.14^{+0.02}_{-0.02}$	$1.18^{+0.01}_{-0.01}$
$\log(mr_{H_2O})$	$\cdots$	-2.311	-1.366	-2.605	-1.655	-4.314	-3.994	$-1.10^{+0.06}_{-0.09}$
$\log(mr_{CO})$	$\cdots$	-2.259	-1.312	-2.258	-1.303	-2.290	-1.322	$-5.91^{+2.45}_{-2.30}$
$\log(mr_{CO_2})$	$\cdots$	-5.988	-4.036	-6.300	-4.337	-8.954	-7.475	$-7.23^{+1.41}_{-1.45}$
$\log(mr_{CH_4})$	$\cdots$	-5.913	-5.957	-5.669	-5.661	-3.913	-3.331	$-7.10^{+1.73}_{-1.58}$

Discussion

5 Discussion

5.1 Comparison to Petrus et al. (2021)

Petrus et al. (2021) conducted a thorough analysis of the joint data set of VLT/SINFONI, SHERE, and NaCo that covers ~1-5 μm. Here we compare our result of the run with the highest evidence to their "K band with continuum" run in their Table 2 .

- **Planet bulk properties such as log(g) and RP** are consistent. Our inferred log(g) and R_P are $3.19^{+0.23}_{-0.25}$ and $1.23^{+0.02}_{-0.02}$ vs. <4.2 and $1.28^{+0.10}_{-0.11}$ in their Table 2. Error bars and systematics for log(g) and R_P in our retrieval analysis can be as high as 0.6 dex and 0.1 $R_{Jupiter}$ for the fixed abundance cases as learned from §3.
- In terms of **chemical properties**, we find that models with solar metallicity, solar C/O (C/O = 0.55) or sub-solar C/O (C/O = 0.40) are the most likely models. This is consistent with the finding in Petrus et al. (2021) that the planet metallicity [M/H] is $0.05^{+0.24}_{-0.22}$ and C/O is lower than 0.50.
- Our retrieved **effective temperature** T_{eff} is $1477^{+8}_{-10}\ K$. In comparison, T_{eff} in Petrus et al. (2021) is $1518^{+88}_{-71}\ K$, which is consistent within 1-σ. Our inferred **planet luminosity** is $\log(L/L_\odot) = -4.167^{+0.003}_{-0.002}$, which is also consistent with the result in Petrus et al. (2021) at $\log(L/L_\odot) = -4.10 \pm 0.2$.

5 Discussion

5.2 Comparison to Carter et al. (2023)

Carter et al. (2023) inferred planet properties using two methods: **fitting evolutionary tracks and atmospheric models**. The two methods return significantly different results.

Fitting evolutionary tracks results in a planet radius of $1.45 \pm 0.03 \; R_{Jupiter}$, log(g) of 3.93 ± 0.07, and T_{eff} of $1282^{+26}_{-31} \; K$.

Fitting atmospheric models results in a planet radius of $0.92 \pm 0.04 \; R_{Jupiter}$, log(g) of 4.07 ± 0.19, and T_{eff} of $1667^{+25}_{-24} \; K$.

They concluded that the result by fitting evolutionary tracks is more physical because a larger planet radius is expected for a young contracting planet.

Our result in this work is different from either of their results. This can be attributed to the different approach: we conduct retrieval analysis whereas Carter et al. (2023) fit the same data set with evolutionary tracks and atmospheric models.

5 Discussion

5.3 Potential future improvement

- While we find strong evidence for silicate clouds, current retrieval analysis does not allow us to make more physical and quantitative statement about the silicate clouds. As pointed out in Molli`ere et al. (2020), using $\log(mr_{MgSiO_3})$, $\log(K_{zz})$, f_{sed}, and σ_g are just "a glorified way" of parameterizing clouds. These parameters, however, are not self-consistently included in the model.

- In addition, while $MgSiO_3$ is the only cloud species that is considered this work, there can be other unaccounted cloud species (e.g., SiO_2, Fe, and Mg_2SiO_4, Burningham et al. 2021) to condensate around ~1500 K, which is the effective temperature of HIP 65426 b.

- §4.4 already discusses the unrealistic chemistry that is inferred from the all-varying run. This can be largely attributed to the lack of data with higher spectral resolution: the JWST and SPHERE data that are used in this work are either **photometric data or IFU data with R lower than ~15**. Including data with higher spectral resolution such as VLT/SINFONI (R~5,500), JWST (e.g., NIRSpec with R up to 3,600), and VLT/HiRISE (R~100,000,) will resolve molecular lines and offer a much better direct measurement and constraint on chemical abundances.

Summary

6 Summary

We perform retrieval analyses on a joint data set of SPHERE and JWST for HIP 65426 b.

- We find that the atmosphere of HIP 65426 b is more likely to have a solar metallicity and a C/O ratio at 0.4 or 0.55 than 10x solar metallicity and a C/O=1.0 based on model comparison using Bayesian evidence.
- The preferred model shows strong evidence of silicate clouds and the presence of silicate clouds is robust against all assumptions that we consider in this work.
- We find no sign of an enshrouding dust for HIP 65426 b that exists in other young planets such as PDS 70 b and c.

Below we summarize our findings from retrieval analyses with low-resolution IFU data and JWST NIRCam and MIRI photometric data points.

- Low-resolution and photometric data points that cover a broad wavelength range can provide a certain level of constraint on metallicity and C/O ratio, e.g. >3-σ to distinguish between 1 dex difference in metallicity (i.e., 1x and 10x solar metallicity) and a few tenths in C/O (§3.3).
- The presence of clouds and the type of cloud can be inferred by comparing the pressure range for the cloud opacity and the pressure range for the flux contribution function (Fig. 2), and by checking the dip of the 11.4 µm photometric data point (Fig. 1 and §4.2).
- Our work suggests using mock data to test the retrieval code and understand the limitations of the actual data set, the mock data set, and the retrieval analysis (§3).

Thanks

闫冰
2023/11/24